

The Production of Sodium and Aluminum in Globular Cluster Red Giant Stars

Robert M. Cavallo

Department of Astronomy, University of Maryland, College Park, MD 20742;
rob@astro.umd.edu

Allen V. Sweigart

Laboratory for Astronomy and Solar Physics, Code 681, NASA/Goddard Space Flight
Center, Greenbelt, MD, 20771; sweigart@bach.gsfc.nasa.gov

and

Roger A. Bell

Department of Astronomy, University of Maryland, College Park, MD 20742;
roger@astro.umd.edu

ABSTRACT

We study the production of Na and Al around the hydrogen shell of two red-giant sequences of different metallicity in order to explain the abundance variations seen in globular cluster stars in a mixing scenario. Using detailed stellar models together with an extensive nuclear reaction network, we have calculated the distribution of the various isotopic abundances around the hydrogen shell at numerous points along the red-giant branch. These calculations allow for the variation in both temperature and density in the shell region as well as the timescale of the nuclear processing, as governed by the outward movement of the hydrogen shell. The reaction network uses updated rates over those of Caughlin & Fowler (1988). We find evidence for the production of Na and Al occurring in the NeNa and MgAl cycles. In particular, Na is significantly enhanced throughout the region above the hydrogen shell. The use of the newer reaction rates causes a substantial increase in the production of ^{27}Al above the hydrogen shell through heavy leakage from the NeNa cycle and should have an important effect on the predicted surface abundances. We also find that the nuclear processing is considerably more extensive at lower metallicities.

Subject headings: Globular Clusters: general - Nuclear Reactions,
Nucleosynthesis, Abundances - Stars: Abundances - Stars: late-type -
Stars: Interiors - Stars: Population II

1. Introduction

Briley et al. (1994) and Kraft (1994) have reviewed the observational data on variations in the abundances of C, N, O, Na, and Al in globular cluster red-giant-branch (RGB) stars. The variations in Na and Al are particularly significant, since they have long been regarded as one of the principal arguments in favor of a primordial origin for the abundance anomalies (see e.g., Cottrell & Da Costa 1981). Star-to-star variations of Na were first observed by Cohen (1978) and Peterson (1980) in M13 and M3, while similar variations of Al, which are correlated with the CN band strength, were found by Norris et al. (1981) in NGC 6752. Since these original observations, numerous other groups have confirmed the general existence of Na and Al vs. N correlations and Na and Al vs. O anticorrelations in globular cluster red giants (Drake et al. 1992; Kraft et al. 1992, 1993). Recently Norris & Da Costa (1995) have concluded that Na variations exist in all clusters, while Al variations are greater in the more metal-poor clusters.

Except for the modest alterations due to the first dredge-up, canonical stellar evolution models predict no changes in the C, N, O, Na, and Al surface abundances during the RGB phase. In an attempt to explain this discrepancy between the predicted and observed abundance variations, Sweigart & Mengel (1979; hereafter, SM79) suggested that meridional circulation currents, driven by internal rotation, might be able to mix material across the radiative zone that separates the top of the hydrogen shell (H shell) from the base of the convective envelope in canonical RGB models. They found that there was a region of significant extent just above the H shell within which the CN cycle has processed C into N and, somewhat closer to the shell, there was a region within which the ON cycle has processed O into N. The mixing was postulated to begin at the point along the RGB where the H shell burns through the hydrogen discontinuity that was previously produced by the deep penetration of the convective envelope during the first dredge-up. A progressive depletion of carbon is seen along the giant branch in M92, M15, and NGC 6397 (Bell, Dickens, & Gustafsson 1979; Carbon et al. 1982; Trefzger et al. 1983; Briley et al. 1990), although the luminosity at which this depletion begins is uncertain, for observational reasons. If Na and Al were also manufactured in the CN- and ON-processed regions, then mixing might also explain the observed Na and Al variations. Complimenting the SM79 hypothesis, Denisenkov & Denisenkova (1990; hereafter, DD90) have suggested ^{23}Na can be produced from proton captures on ^{22}Ne in the ON-processed region and that the rotation rate required by SM79 is sufficient to reconcile the observations with theory.

Expanding on the concepts of SM79 and DD90, Langer, Hoffman, & Sneden (1993; hereafter, LHS93; see also Langer & Hoffman 1995 and Denissenkov & Weiss (1996)) examine the production of Na and Al in RGB stars by following the reactions of the relevant

nuclei in a simplified model with a low metallicity ($Z = 0.0001$ or $[\text{Fe}/\text{H}] = -2.3$) and a constant temperature ($T_9 = 0.040$ where $T_9 = T/10^9\text{K}$) and density ($\rho = 44.7 \text{ g cm}^{-3}$). Their study shows a significant enhancement of ^{23}Na in the ON-processed region which derives from a series of proton captures on ^{20}Ne in the NeNa cycle. Furthermore, their model yields an increase in ^{27}Al which is made from proton captures on both ^{25}Mg and ^{26}Mg via the reactions $^{25}\text{Mg}(p, \gamma)^{26}\text{Al}(\beta^+)^{26}\text{Mg}(p, \gamma)^{27}\text{Al}$. Their study also shows that a MgAl cycle is set up after 1.7 Myr. This cycle begins with a proton capture on ^{24}Mg , which is itself enhanced through leakage from the NeNa cycle by a (p, γ) reaction with ^{23}Na , and is completed with $^{27}\text{Al}(p, \alpha)^{24}\text{Mg}$. Both the NeNa and MgAl cycles are depicted graphically in Figure 1.

The purpose of this *Letter* is to develop the work of LHS93 further by using detailed stellar evolutionary sequences to examine the production of Na and Al around the H shell in RGB stars. This represents an improvement over LHS93 because: 1) we incorporate the latest reaction rates in our burning code, 2) we explore a wider parameter space in both metallicity and luminosity, and 3) our more realistic RGB models take into account the variation in temperature and density around the H shell and incorporate the timescale for the nuclear processing to produce Na and Al, as set by the rate at which the H shell moves outward in mass. The Na and Al produced in this fashion can then be mixed outward into the envelope over the relevant timescale for the mixing process. Section 2 summarizes our numerical techniques and input physics while section 3 presents the results of our calculations for some representative cases. We conclude with a brief discussion of our results in section 4.

2. Sequences and Network

In this *Letter* we present results for two RGB sequences, one with mass $M = 0.795 M_\odot$ and scaled-solar metallicity $Z = 0.0001$, and one with $M = 0.875 M_\odot$ and $Z = 0.004$. Each of these sequences was evolved from the zero-age main sequence up the giant branch to the onset of the helium flash. The masses were chosen to give an age of 15 Gyr at the helium flash. We began our calculation of the abundance distributions around the H shell at the point on the RGB where the H shell burns through the hydrogen discontinuity produced during the first dredge-up. This occurs at a luminosity of $\log(L/L_\odot) = 2.28$ and 1.72 in the low and high metallicity sequences, respectively. Above this luminosity, mixing into the nuclearly processed region at the top of the H shell is no longer hindered by a gradient in the mean molecular weight. Calculations of the abundance distributions were carried out in increments of $0.005 M_\odot$ in the helium-core mass until the models reached the helium flash.

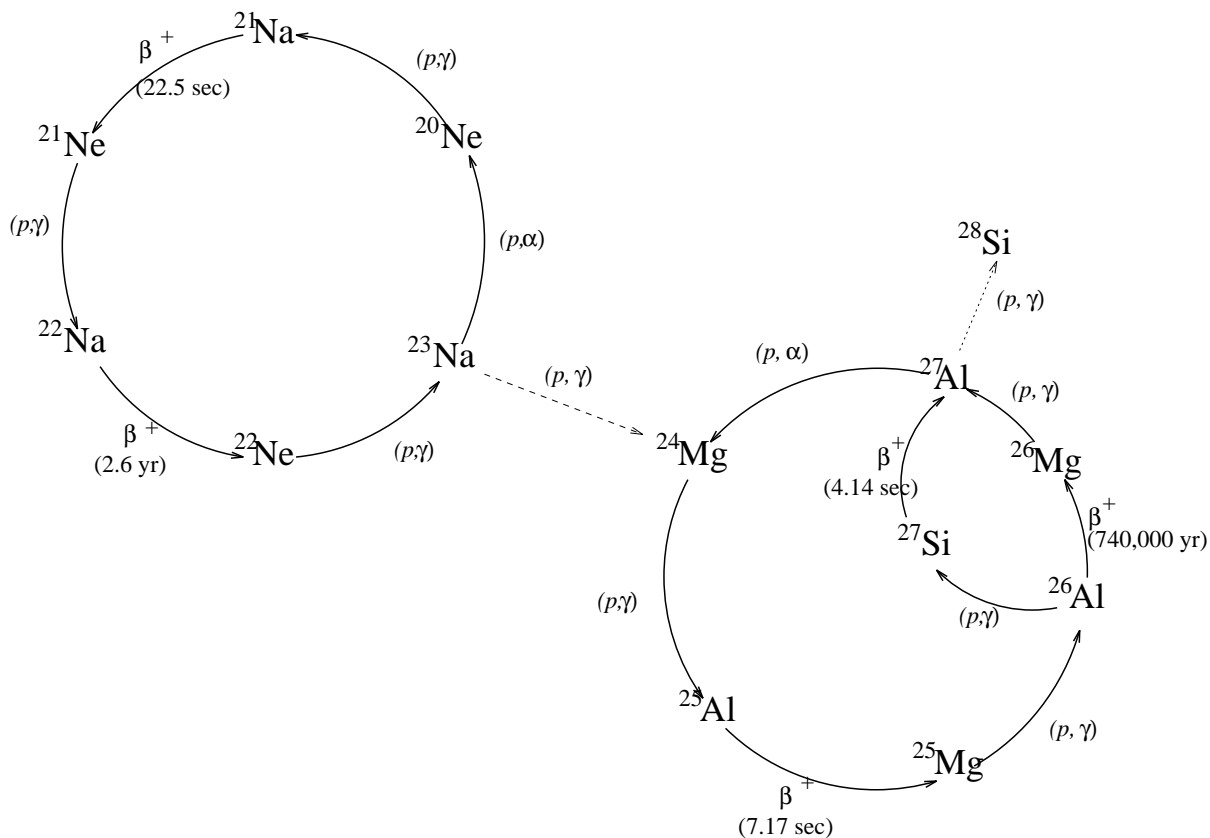


Fig. 1.— The reactions involved in the NeNa and MgAl cycles. The half-lives and reaction types are given parenthetically. In the case of competing decay paths, the solid lines show the stronger path, derived with the rates used in our code for the relevant temperature range. The dashed lines show the weaker decays which lead to a depletion in the total abundance of each cycle (“leakage”).

Typical temperatures and densities within the nucleary processed region were in the range from $0.015 < T_9 < 0.06$ and $0.3 < \log(\rho) < 2.5$.

Our nuclear reaction network code was kindly supplied to us by Dr. David Arnett. The majority of the reaction rates are taken from Caughlin & Fowler (1988; hereafter, CF88). When available, we include the more recent rates for the NeNa and MgAl cycles as reviewed by Arnould, Mowlavi, & Champagne (1995; hereafter, AMC95). In particular, we include the latest results for the Ne and Na proton capture rates by El Eid & Champagne (1995). The Mg and Al proton capture rates are obtained from Iliadis et al. (1990) and Champagne, Brown, & Sherr (1993). AMC95 re-evaluate the ^{27}Al proton capture decay paths and find, contrary to the results of Timmermann et al. (1988) and Champagne et al. (1988) but in agreement with CF88, that the α -decay channel is stronger than the γ -decay channel, so that the MgAl reaction rates do, in fact, lead to cycling.

The network code requires a run of temperature and density, which are given by the models, and a timestep, which we supply using the stationary shell approximation (see e.g. Sweigart 1994). This approximation shows excellent agreement with the conventional solution of the differential equations for the CNO reactions (Clayton 1983) and will be discussed more fully in a future publication. The initial abundances for the main CNO isotopes outside the H shell are obtained from the RGB models. We input the initial values for the other elements from ^{19}F to ^{44}Ca according to their scaled solar values (Anders & Grevesse 1989).

3. Results and Discussion

3.1. Results Using Updated Reaction Rates

Figure 2 shows the elemental profiles around the H shell of the low metallicity sequence at the start of mixing and at the onset of the helium flash. Panels a and b clearly demonstrate the initial rise in ^{23}Na from ^{22}Ne throughout a region above the H shell, as predicted by DD90, followed by the cycling of ^{20}Ne into ^{23}Na somewhat closer to the shell, as discussed by LHS93. This rise in ^{23}Na occurs within the region of C depletion which extends out to $\Delta M_r = 0.0040$ and 0.0015 in panels a and b, respectively. The lower panels highlight the MgAl cycle. As one progresses inward toward the H shell in panel c, ^{26}Al is produced first from ^{25}Mg and then converted into ^{27}Al through the paths shown in Figure 1. With advancement up the RGB, some ^{27}Al is eventually destroyed via $^{27}\text{Al}(p, \alpha)^{24}\text{Mg}$. By the tip of the RGB, the NeNa cycle (panel b) is leaking heavily into the MgAl cycle and producing sizable enhancements in ^{27}Al just above the H shell (panel d). This huge

increase in ^{27}Al happens during the last 15% of the RGB lifetime, possibly allowing enough time for mixing to the surface.

For comparison, Figure 3 shows the same abundance profiles for the $M = 0.875 M_{\odot}$, $Z = 0.004$ sequence. Since the temperature around the H shell is lower in this sequence, the changes in the abundances are less dramatic throughout the evolution up the RGB, when compared to the low metallicity sequence. Nevertheless, ^{23}Na is still enhanced in a region above the shell, especially at the start of mixing (panel a). Significant production of ^{27}Al , however, is only seen in panel d and even then only within the H shell. A similar decrease in the extent of the CN- and ON-processed regions in RGB models of higher metallicities was found by SM79 . Thus mixing in more metal-rich globular cluster giants should have less effect on the surface abundances, especially in the case of Al. Some of these rough estimates seem to be confirmed by Norris & Da Costa (1995), who note that the ω Cen giants with low $[\text{Fe}/\text{H}]$ show a greater production of Al relative to Na.

3.2. Comparison with the Caughlin & Fowler (1988) Reaction Rates

In order to study the effects of using updated reaction rates, we recalculated our profiles using the older CF88 rates. These are plotted in Figure 4 for the low metallicity sequence. The patterns indicative of NeNa and MgAl cycling are clearly visible. The most notable difference from the previous results is in the enhancement of ^{27}Al at the onset of the helium flash. With the CF88 rates (Figure 4d), the increase of ^{27}Al at the center of the H shell is a factor of two lower than with the newer rates (Figure 2d). Further, the large increases in Al only occur during the last 5% of the RGB lifetime. With the CF88 rates, the NeNa cycle does not leak as heavily into the MgAl cycle, resulting in a larger build-up of ^{23}Na (Figure 4b vs. Figure 2b) and a smaller enhancement of ^{24}Mg . This effect is offset, however, by the fact that the region of ^{23}Na enhancement extends further above the H shell with the new rates. Since mixing is postulated to occur only above the H shell, one expects the more modern rates to increase the predicted surface abundances of Na and Al.

4. Conclusion

By combining our realistic stellar models with an updated nuclear reaction network, we are able to follow the nucleosynthesis of C, N, O, Ne, Na, Mg, and Al around the H shell of two sequences of differing metallicity as they evolve up the RGB. In qualitative agreement with the observations, our results show an increase in ^{23}Na above the H shell

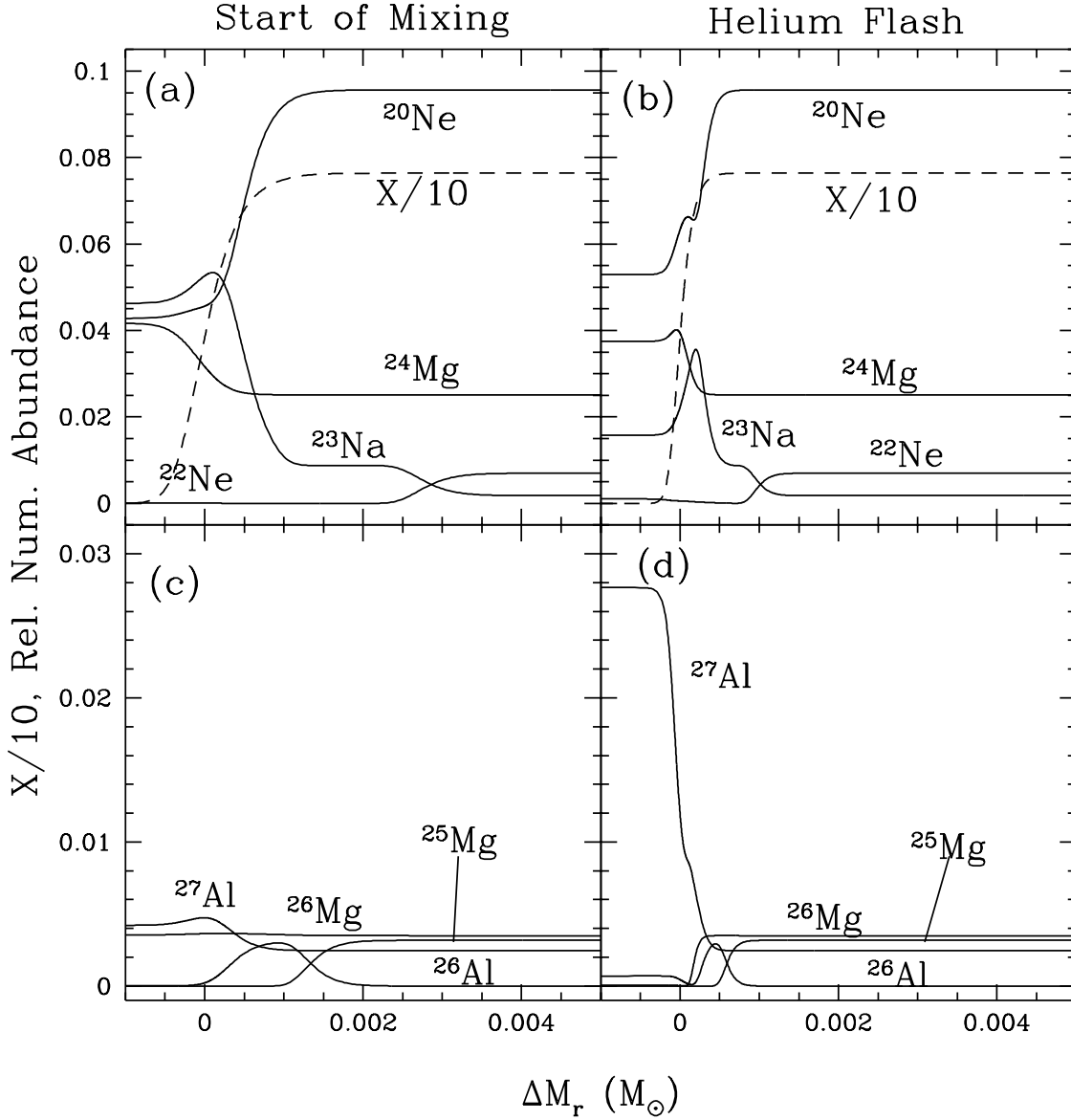


Fig. 2.— Abundance profiles around the H shell for the sequence with $M = 0.795 M_{\odot}$ and $Z = 0.0001$ at the start of mixing (left panels) and at the onset of the helium flash (right panels). The abscissa is the difference in mass from the center of the H shell while the ordinate is the number abundance relative to all metals. The hydrogen mass fraction, scaled to 0.1 of its actual value, is given by the dashed line in the upper two panels. The region of hydrogen depletion defines the H shell.

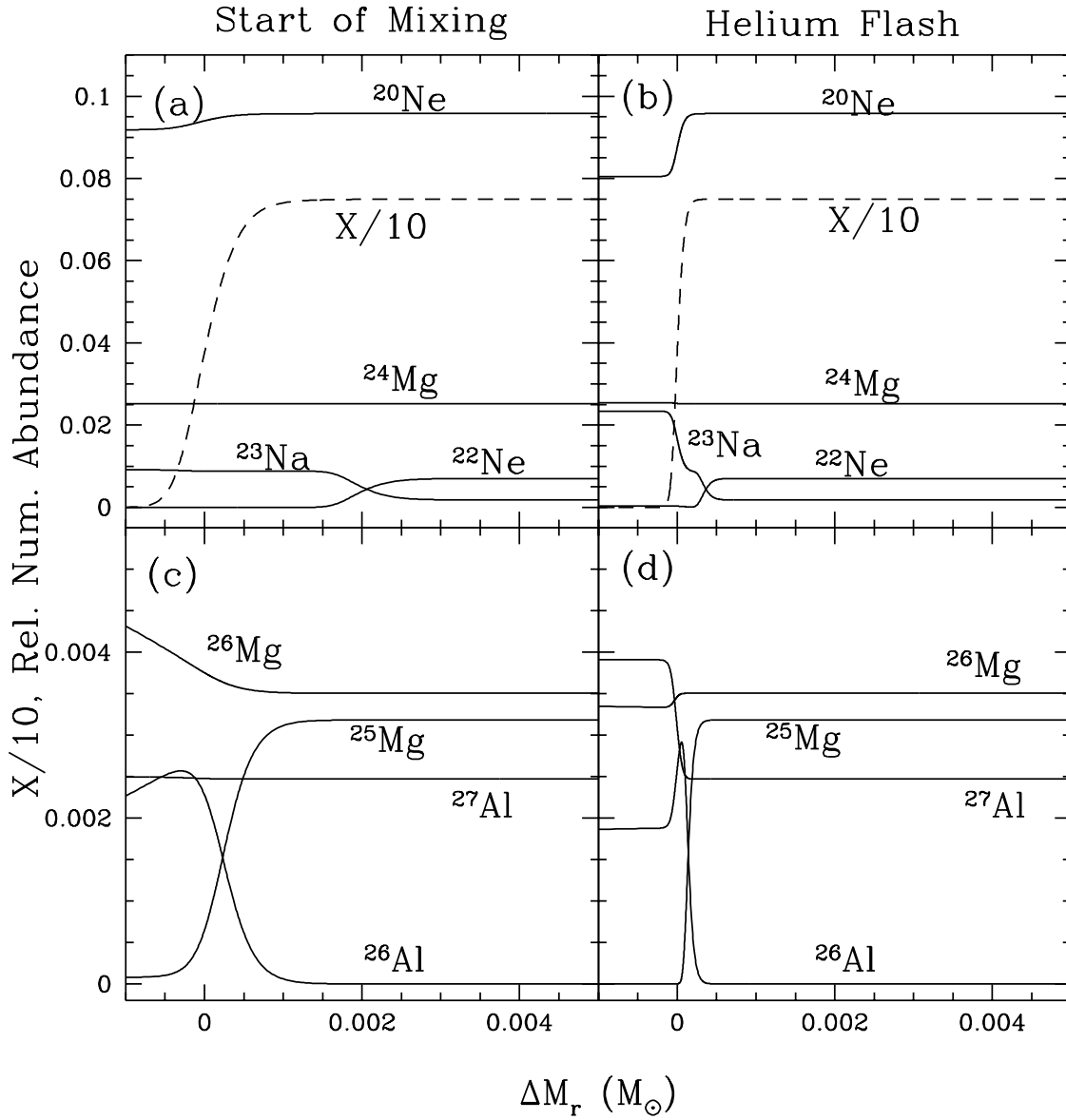


Fig. 3.— As Figure 2, with $M = 0.875 M_\odot$ and $Z = 0.004$.

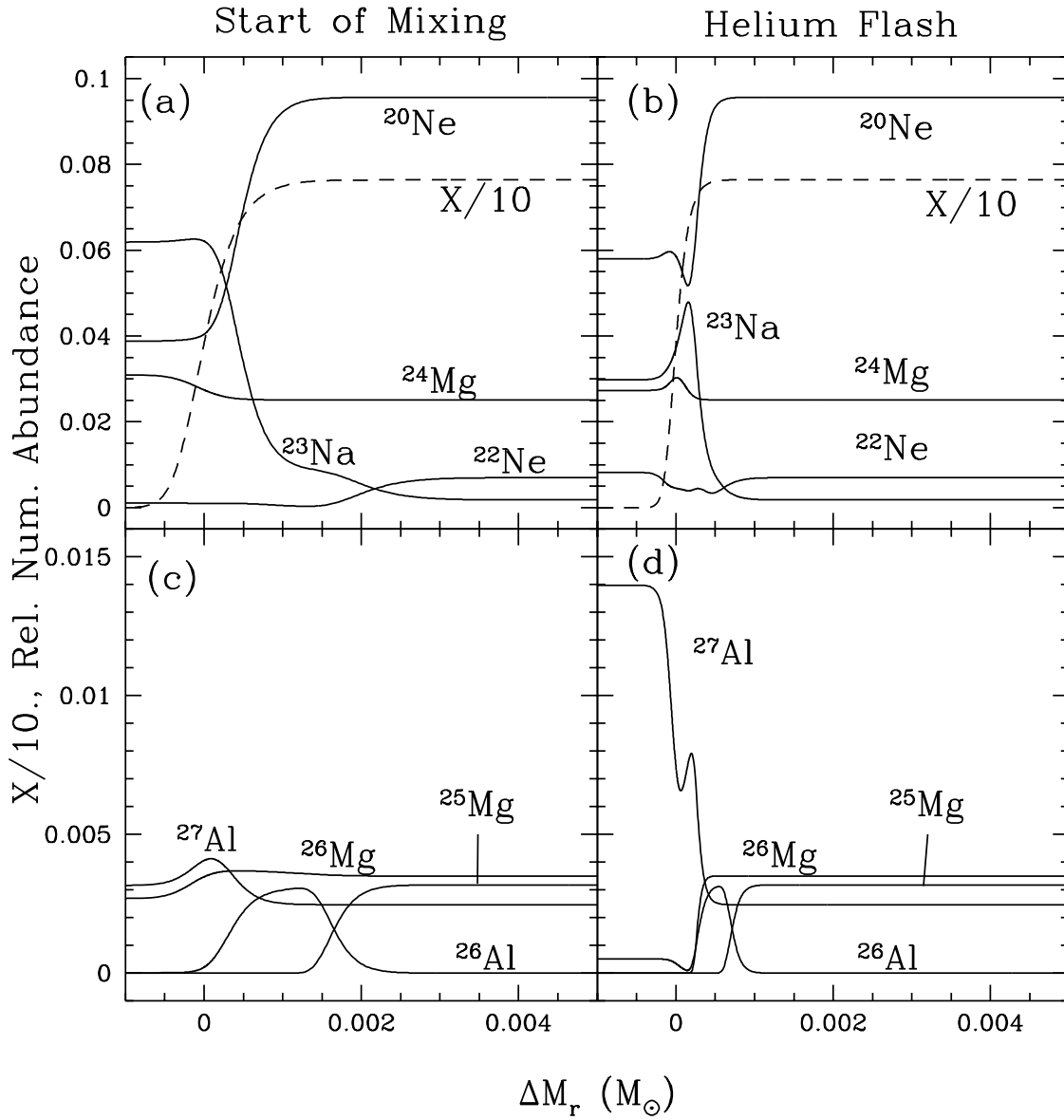


Fig. 4.— As Figure 2, with the older rates of CF88. Note the difference in the vertical scale in panels c and d when compared to figure 2.

throughout the entire giant branch, independent of metallicity. Furthermore, we produce sizable enhancements of ^{27}Al for the low metallicity sequence as it approaches the tip of the RGB, without having to increase the initial $^{25,26}\text{Mg}$ abundance or the ^{26}Mg proton capture rate as in Langer & Hoffman (1995). Thus, our results can potentially reconcile the Na and Al abundance anomalies observed in globular cluster giants with the mixing of these elements from the stellar interior.

Although our work is based on up-to-date reaction rates, those rates can still be quite uncertain in some cases. For example, our results deviate from the observations in the case of ^{24}Mg . Contrary to the findings of Shetrone (1996), who observes a decrease in ^{24}Mg with increasing luminosity in M13 giants, we show an enhancement of ^{24}Mg with continuing evolution for the low metallicity sequence. However, the high metallicity sequence shows only a marginal increase in the ^{24}Mg abundance. Thus, our present inability to qualitatively reproduce the ^{24}Mg observations might be due to the current uncertainty in the nuclear cross-sections. Perhaps a faster rate for the $^{24}\text{Mg}(p, \gamma)^{25}\text{Al}$ reaction or a slower rate for the $^{27}\text{Al}(p, \alpha)^{24}\text{Mg}$ reaction would decrease the ^{24}Mg abundance. Figures 2 and 4 show how the ^{24}Mg abundance can depend on the choice of reaction rates.

In addition to depending on the accuracy of the nuclear reaction rates, any final predictions of surface abundances will also depend strongly on the choice of a mixing mechanism. The mixing timescale, the depth of the mixing, and the dependence on metallicity will all affect the quantitative results for the surface abundances. In a future paper, we will explore these aspects of the mixing mechanism and will compare the predicted variations of the surface abundances along the RGB with the observational constraints.

In order to better understand the effects of metallicity, we will also extend the present work to a Population I red giant. Furthermore, we will use the same set of sequences to study the CNO isotopes. Finally, we intend to follow the production and destruction of ^3He along the RGB in order to determine better how low mass stars affect the chemical evolution of this isotope in the Galaxy.

The authors wish to thank Dr. David Arnett of the University of Arizona for the use of his fine nuclear reaction network and for his immeasurable patience in helping us implement the code. We also wish to thank Drs. M. Arnould, N. Mowlavi, and A. Champagne for allowing us to preview their work on the uncertainties in our reaction rates. The work of A.V.S. is funded in part by NASA RTOP 188-41-51-03 and that of R.A.B. by NSF AST93-14931. Finally, R.M.C. wishes to acknowledge the NASA Graduate Student Research Program for financial support of his research.

REFERENCES

- Anders, E. & Grevesse, N. 1989, *Geochim. Cosmochim. Acta*, 53, 197
- Arnould, M., Mowlavi, N., & Champagne, A. 1995, to appear in *Stellar Evolution: What Should Be Done*, 32nd Liege Int. Astroph. Coll.
- Bell, R. A., Dickens, R. J., & Gustafsson, B. 1979, *ApJ*, 229, 604
- Briley, M. M., Bell, R. A., Hesser, J. E., & Smith, G. H. 1994, *Can. J. Phys.*, 72, 772
- Briley, M., Bell, R. A., Hoban, S., & Dickens, R. J. 1990, *ApJ*, 259, 307
- Carbon, D. F. et al. 1982, *ApJS*, 49, 207
- Caughlin, G. R. & Fowler, W. A. 1988, *Atom. Data and Nuc. Data Tables*, 40, 283
- Champagne, A. E., Brown, B. A., & Sherr, R. 1993, *Nucl. Phys. A*, 556, 123
- Champagne, A. E. et al. 1988, *Nucl. Phys. A*, 487, 433
- Clayton, D. D. 1968, *Principles of Stellar Evolution and Nucleosynthesis* (New York: McGraw-Hill)
- Cohen, J. G. 1978, *ApJ*, 223, 487
- Cottrell, P. L. & Da Costa, G. S. 1981, *ApJ*, 245, L79
- Denisenkov, P. A. & Denisenkova, S. N. 1990, *Sov. Astron. Lett.*, 16, 642
- Denissenkov, P. A. & Weiss, A. 1996, preprint
- Drake, J. J., Smith, V. V., & Suntzeff, N. B. 1992, *ApJ*, 295, L95
- El Eid, M. F. & Champagne, A. E. 1995, *ApJ*, 451, 298
- Iliadis, Ch. et al. 1990, *Nucl. Phys. A*, 512, 509
- Kraft, R. P. 1994, *PASP*, 106, 553
- Kraft, R. P., Sneden, C., Langer, G. E., & Prosser, C. F. 1992 *AJ*, 104, 645
- Kraft, R. P., Sneden, C., Langer, G. E., & Shetrone, M. D. 1993 *AJ*, 106, 1490
- Langer, G. E., Hoffman, R., & Sneden, C. 1993, *PASP*, 105, 301
- Langer, G. E. & Hoffman, R. D. 1995, *PASP*, 107, 1177
- Norris, J., Cottrell, P. L., Freeman, K. C., & Da Costa, G. S. 1981, *ApJ*, 244, 205
- Norris, J. E. & Da Costa, G. S. 1995, *ApJ*, 441, L81
- Peterson, R. C. 1980, *ApJ*, 237, L87
- Shetrone, M. D. 1996, *BAAS*, 27, 1432

Sweigart, A. V. 1994, ApJ, 426, 612

Sweigart, A. V. & Mengel, J. G. 1979, ApJ, 229, 624

Timmermann, R., Becker, H. W., Rolfs, C., Schröder, U., & Trautvetter, H. P. 1988,
Nucl. Phys. A, 477, 105

Trefzger, C. F., Carbon, D., Langer, G. E., Suntzeff, N. B., & Kraft, R. P. 1983, ApJ, 266,
144